Chapter 4

Photon heating of envelopes around young stellar objects:

An explanation for CO J=6–5 emission

Abstract

We propose that the narrow ^{12}CO and ^{13}CO J=6–5 emission observed toward many low-mass young stellar objects is produced in molecular material in the circumstellar envelope which is heated by the 10,000 K radiation field generated in the inner part of the accretion disk. Ultraviolet photons traveling through the biconical cavity evacuated by the bipolar outflow are scattered by dust grains present in the low density material in the cavity. These photons are not energetic enough to photodissociate H_2 and CO, but can heat the envelope surrounding the cavity. The temperature structure and the CO excitation of this photon-dominated region are computed using two-dimensional Monte Carlo methods. It is found that the material is heated up to a few hundred K close to the cavity wall, and that the observed low-velocity mid-J CO emission can be well explained by our model for a wide range in envelope density and stellar luminosity. Emergent CO spectra are compared to observations of the embedded low-mass young stellar object TMR 1.

4.1 Introduction

Until recently, ^{12}CO 6–5 emission at 690 GHz from young stellar objects (YSOs) had been observed in only a few sources with particularly strong lines, and this emission was proposed to originate in shocked gas associated with the outflow (Schuster et al. 1993). Improvements in the sensitivity of high-frequency receivers now make the detection of weaker ^{12}CO and ^{13}CO 6–5 emission possible. A recent survey of 13 low-mass embedded objects in the Taurus and Serpens regions performed in Chapter 3 (Hogerheijde et al. 1998a) indicates that the ^{13}CO 6–5 emission is narrow with typical main beam temperatures of 0.5–5 K, and exhibits relatively little variation from source to source. The excitation of the J=6 level of CO requires densities of $n_{\mathrm{H}_2} > 10^5$ cm^{-3} and temperatures of $\sim$ 100 K. While some of this emission is clearly associated with the bipolar outflows driven by these objects as indicated by the presence of strong wings in the ^{12}CO lines, a considerable fraction of the ^{12}CO emission, and most of the ^{13}CO emission, is found within $\pm$2 km s^{-1} of ambient cloud velocity. Therefore, it is unlikely that all of this mid-J CO emission is generated in J-shocks driven by the bipolar outflow: even an oblique shock would have to be very inefficient in accelerating material

Spaans, Hogerheijde, Mundy, & van Dishoeck 1995, ApJL, 455, L167

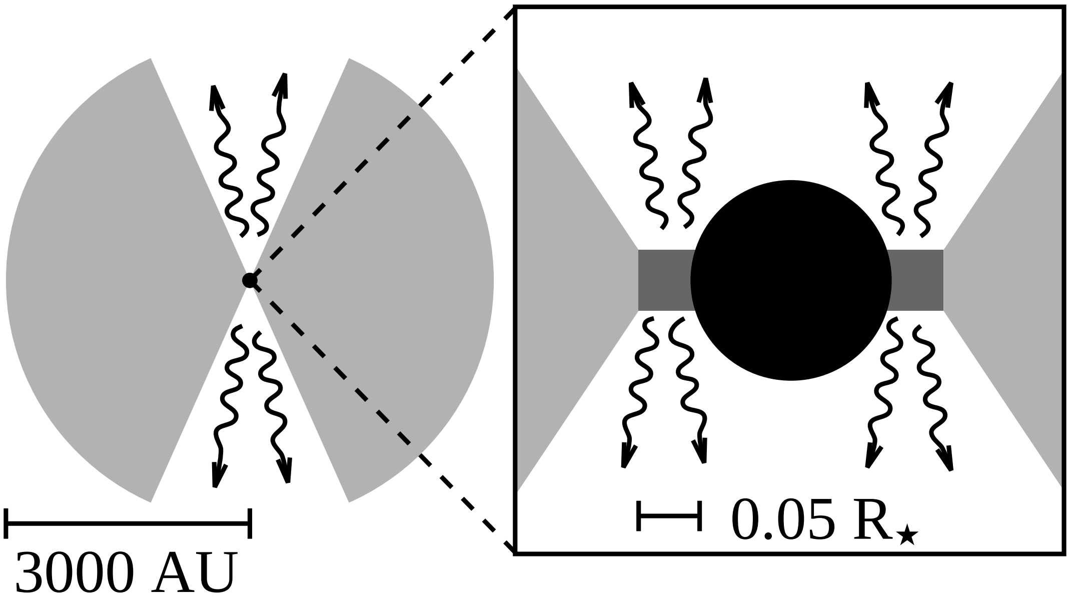

Fig. 4.1. *Sketch of the adopted model for the cavity region around the YSO.*

to limit the line width to $\Delta V \approx$ 2–3 km s^{-1} for typical shock velocities of $\sim$ 80 km s^{-1} or more. Only low-velocity C-shocks with V_s = 5–10 km s^{-1} could result in similarly narrow lines (Draine & Roberge 1984).

Here we propose a mechanism for heating the molecular material by ultraviolet photons originating at the boundary layer between accretion disk and protostellar object. These energetic photons are scattered into the surrounding envelope by the small amount of dust present in the cavity (see Fig. 4.1), creating conditions reminiscent of the cool photon-dominated regions (PDRs) around late-type stars studied by Spaans et al. (1994). The scattering of the ultraviolet radiation, the heating of the gas, and the molecular excitation are modeled using a two-dimensional Monte Carlo method developed by Spaans (1996). The molecular material is dense and warm enough to excite the mid-J CO lines. The resulting emission-line spectra are calculated, and compared to observations of ^{12}CO 6–5 and 4–3, and ^{13}CO 6–5 and 3–2 obtained toward the embedded low-mass YSO TMR 1.

4.2 Basic model

The source is modeled as a circumstellar molecular envelope, a central protostar with a geometrically thick (§4.2.2) accretion disk, and a hot boundary layer where a significant fraction of the gravitational potential energy is dissipated. It is assumed that there is a biconical cavity cleared by the outflow through which the ultraviolet photons generated at the boundary layer can escape (see Fig. 4.1).

4.2.1 The circumstellar envelope

The spherical molecular envelope is modeled following the collapse solution of Shu (1977) and Terebey, Shu, & Cassen (1984), in the regime where the collapse expansion wave has propagated well outside the region of interest. In this case, the density distribution follows a power law in radius with an index of -1.5: $n_{\mathrm{H}_2}(r) = n_0(r/r_0)^{-1.5}$. Typical values for n_0 range between 10^4 cm^{-3} and 10^6 cm^{-3} at a characteristic radius of $r_0 =$ 1000 AU. The effects of rotation, which are generally small (cf. Chapter 7), are neglected here. The envelope extends from an inner radius of 50 AU to an outer radius of 3000 AU where the envelope fades into the quiescent surrounding cloud. The assumption of collapse is not essential in our model to reproduce the integrated CO line emission, although it influences the exact shape of the line profiles.

4.2.2 The central protostar, accretion disk and boundary layer

A protostar surrounded by a geometrically thick accretion disk, i.e., with a thickness of at least 0.2 times its diameter, is assumed present at the center of the spherical envelope. A large fraction of the gravitational energy of the accreting material is dissipated in the boundary layer between the fast-rotating accretion disk and the protostar, which rotates at a much lower rate well below break-up. The radiation field of this boundary layer is represented by a blackbody with effective temperature $T_{\mathrm{rad}} = 10,000$ K, motivated by observations of spectral veiling and ultraviolet excess of T Tauri stars (Basri & Batalha 1990; Hartigan et al. 1991). It is assumed that a similar boundary layer exists around the embedded objects studied here. Because the boundary layer is expected to be optically thick and nearly isothermal, the blackbody approximation should be a reasonable one. Nevertheless, the detailed spectral properties of the emission are strongly influenced by chromospheric action in the form of acoustic and magnetic waves and their subsequent dissipation (Kenyon & Hartmann 1987).

The width of the annular boundary layer d_{bl} follows from the condition that the luminosity L_{bl} from both faces equals $2\pi\sigma \int T_{\mathrm{rad}}^4 r dr$, where the integral runs from $R_\star$ to $R_\star + d_{\mathrm{bl}}$. We constrain L_{bl} as a fraction η of the total bolometric luminosity, $L_{\mathrm{bl}} = \eta L_{\mathrm{bol}}$. The remaining $(1-\eta)L_{\mathrm{bol}}$ is generated in the protostar and the accretion disk. A value of $\eta = 0.3$ is adopted (Basri & Bertout 1993). The resulting size of the boundary layer for a 1 $L_\odot$ protostar is approximately 2×10^{10} cm, in good agreement with the range given by Hartigan et al. (1991) of $0.01 < d_{\mathrm{bl}}/R_\star < 0.1$ for a 5 $R_\odot$ protostar. Each face of the annulus radiates isotropically into the forward 2π steradians. The radiation field of the boundary layer is truncated at some maximum angle θ_{max}, corresponding to absorption by the thick accretion disk. This θ_{max} is assumed equal to the opening angle θ_c of the biconical cavity. Therefore, no radiation impinges directly on the surrounding envelope.

4.2.3 The outflow cavity

The bipolar outflow driven by the central source is assumed to have cleared a biconical region of opening angle θ_c. A small amount of outflow or wind material is present in this cavity with $n_{\mathrm{H}} \approx 300$–$3000$ cm^{-3}, corresponding to a total visual extinction along the outflow axis of $A_{\mathrm{V}} \approx 0.01$–$0.1$ mag. The material outside the cavity is assumed to be unperturbed by the outflow. In reality some entrainment of molecular material into the outflow or milder acceleration of material along the cavity walls is expected (cf. Chapter 7). A turbulent velocity width of ~ 1 km s^{-1}, substantially larger than the thermal width of ~ 0.3 km s^{-1}, is used to incorporate these processes in an approximate manner.

4.2.4 The photon-dominated region

The envelope is modeled as a two-dimensional PDR exposed to a cool radiation field with $T_{\rm rad} = 10,000$ K (Spaans et al. 1994; Spaans 1996). The protostar forms deep inside a molecular cloud, where most carbon is in CO and hydrogen in H_2. Since the cool 10,000 K radiation field cannot photodissociate H_2 or CO, the abundances stay constant throughout the PDR at ^{12}CO/[H]=10^{-4} and H_2/[H]=0.5. For the other species, values of O/[H]=10^{-4}, C/[H]=10^{-5} and C^+/[H]=10^{-7} are adopted.

A standard gas-to-dust mass ratio of 100:1 is assumed and the grain properties listed in Roberge et al. (1991) are adopted for the dust in the cavity. The two-dimensional Monte Carlo code described in Spaans (1996) is used to solve the continuum radiative transfer equation at 31 wavelengths in the interval $\lambda = (0.29 \pm 0.15)/T_{\rm rad}$ cm, i.e., 1400–4400 Å for $T_{\rm rad} = 10,000$ K. The adopted grid size is 70×70, corresponding to a spatial resolution of 45 AU.

The photons heat the gas through the photoelectric effect; other minor sources such as cosmic-ray heating are also included. The contribution due to very small grains and large molecules like PAHs increases relative to that of classical grains in cooler radiation fields. The former remain negatively charged more efficiently and have a correspondingly lower work function (Bakes & Tielens 1994; Spaans et al. 1994). At the relevant densities of $n_{\rm H_2} \approx 10^4$ to a few$\times 10^6$ cm^{-3} the smallest grains in the size distribution with less than 10^5 carbon atoms could be removed by grain coagulation (Kim, Martin, & Hendry 1994; Chokshi, Tielens, & Hollenbach 1993). This decreases the photoelectric heating rate by ~ 50%, well within the uncertainty of the abundances of the major coolants O and CO. The amount of carbon in PAHs and very small grains is assumed equal to 10% of the gas-phase carbon abundance. The larger grains are likely covered by ice mantles, but this does not appear to inhibit photoelectric heating as evidenced by the general presence of warm PDRs in many dense molecular clouds.

The protostar, with an effective temperature of $\sim$ 3000–5000 K, emits very soft photons and its contribution to the photoelectric heating is neglected. Typical enhancements of the boundary layer radiation field over the average interstellar field at 2000 Å are ~ 1000 along the cavity wall (see Fig. 4.2).

The cooling processes include [O I] 63 and 146 μm emission, and the lowest 20 rotational lines of CO. Since most carbon is in CO, the influence of [C II] 158 μm emission on the cooling rates is negligible, contrary to the cool PDRs studied by Spaans et al. (1994). The CO and O level populations are solved for in statistical equilibrium, including excitation by far-infrared radiation from dust, the 2.7 K background radiation field, and optical depth effects assuming a Doppler parameter $b = 1$ km s^{-1} (Spaans 1996). A velocity correlation length of 20% of the extent of the cavity is assumed to account for the presence of systematic velocities due to infall.

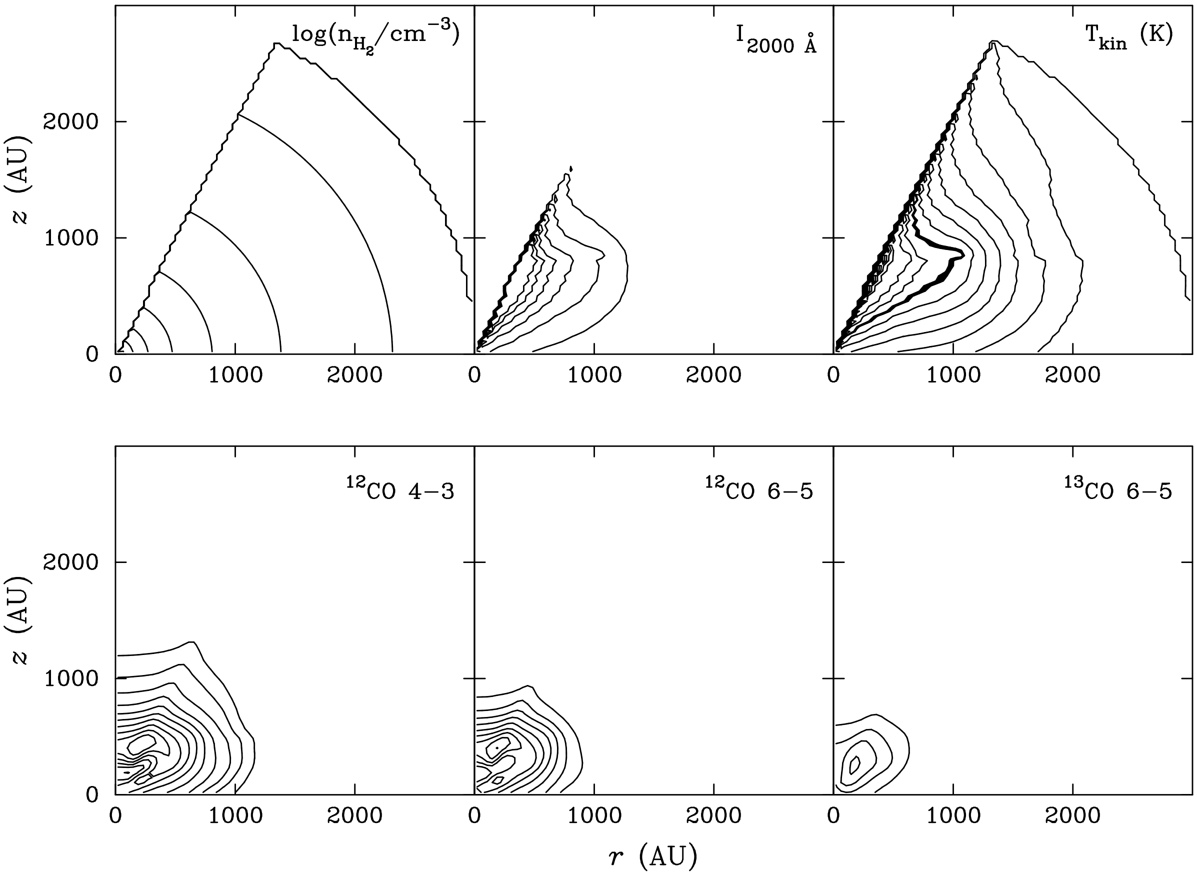

Fig. 4.2. *Results for the generic model with $L_{\rm bl}$ =1 $L_\odot$, $A_{\rm V}$ =0.1 mag, θ_c =45°, b =1 km s^{-1}, $n_0 = 3.5\times10^4$ cm^{-3} at r_0 =1000 AU, and $T_{\rm rad}$ =10,000 K. (top, left) H_2 number density of the adopted model. Three contour levels are drawn per decade; levels start at 5×10^4 cm^{-3}. (middle) Average intensity at 2000 Å. Levels are drawn at 200, 400, ... times the average interstellar radiation field. (right) $T_{\rm kin}$. Levels are drawn at 10, 20, 30, ... K. (bottom, left) ^{12}CO 4–3 , (middle) ^{12}CO 6–5, and (right) ^{13}CO 6–5 peak line intensity maps for an edge-on line of sight, convolved with a 140 AU FWHM beam. For ^{12}CO contours start at 4 K and increase with steps of 4 K; for ^{13}CO 0.4 K intervals are shown.*

4.3 Temperature structure and CO emission

The general characteristics of the resulting temperature distribution are illustrated by a generic model with $L_{\rm bl} = 1\ L_\odot$, $A_{\rm V} = 0.1$ mag in the outflow region, a cone-shaped geometry with opening angle $\theta_c = 45°$, a density $n_0 = 3.5 \times 10^4$ cm^{-3} at 1000 AU, and effective temperature of $T_{\rm rad} = 10,000$ K.

Figure 4.2 presents the density structure, the angle averaged radiation field at 2000 Å in units of the interstellar radiation field strength, and the resulting temperature distribution. Only the upper right quadrant of the generic model is shown. A broad region with $T_{\rm kin} \approx 100$ K is readily obtained. The temperature closely follows the radiation field, but the power-law density distribution influences the extent of the warm region. Note that the warmest region is not closest to the disk, because the radiation does not directly impinge on the envelope and is scattered predominantly forward. Also, the density, and hence the cooling rate, is highest close to the disk. The maximum dust temperature for this model is 40 K and decreases outward to approximately 20 K.

The emergent CO line emission spectra are determined by integrating along a large number of lines-of-sight through the PDR model rotated about the outflow axis, and by convolving with a Gaussian beam. The radiative transport is solved by taking small depth steps and adding the local contributions to the intensity and the opacity at each velocity in the line profile. The source can be oriented at any inclination angle with respect to the line-of-sight, and a velocity field can be included containing a turbulent component of width b and a systematic component of the form $V = V_0(r/r_0)^{-0.5}$, corresponding to the Terebey et al. (1984) collapse model.

Figure 4.2 also shows ^{12}CO 4–3 and 6–5, and ^{13}CO 6–5 line maps for the generic model with $V_0 = 1$ km s^{-1} at $r_0 = 1000$ AU and $b = 1$ km s^{-1}, convolved to a resolution of 140 AU ($1''$ at the distance of the Taurus star forming region). The ^{12}CO 6–5 line with an excitation energy of 116 K is confined to a narrow region where the temperature and density are high. The intensity of the ^{12}CO 4–3 line, at 55 K, is less strongly determined by the local density and temperature, and has a broader appearance. Typical line optical depths for these transitions are much larger than unity. The ^{13}CO 6–5 line has a distribution similar to the main isotope line, but with much smaller optical depth.

Additional calculations have been performed with varying boundary layer luminosity. Between $L_{\rm bl} = 0.5\ L_\odot$ and $L_{\rm bl} = 12\ L_\odot$, the total change in maximum kinetic temperature was only 20%. The resulting ^{12}CO and ^{13}CO 6–5 antenna temperatures varied by approximately 50%. These results are encouraging considering the uncertainties in the boundary layer luminosities, and the range of bolometric luminosities in observed YSOs. The main reason that the mid-J CO lines do not depend strongly on boundary layer luminosity is that the [O I] 63 μm line acts as an efficient gas temperature regulator. Consequently, only the total column of warm gas varies with $L_{\rm bl}$. After beam convolution only a moderate dependence follows for the CO emission lines.

Variations in opening angle θ_c of the biconical cavity have no strong impact on the model results. The ultraviolet flux entering the cavity decreases for a smaller opening angle since the radiation field is truncated at this same angle by the thick accretion disk. However, a larger fraction of the ultraviolet photons is scattered into the envelope by the predominantly forward scattering grains. For well-collimated cavities, with $\theta_c \approx 30°$, the radiation field at any given wavelength impinging on the cavity wall is within a factor of two from that of the $\theta_c \approx 90°$ case.

For grains which are more forward scattering, like grain model 3 of Roberge (1990), a smaller fraction of the photons emitted by the boundary layer is scattered into the envelope. The resulting decrease in ultraviolet flux impinging on the envelope is less than the uncertainty in the total amount of scattering material in the outflow cavity. The size of the 100 K region varies by approximately 50% for different grain scattering properties and albedo.

The model results are, however, sensitive to the adopted density structure, because the heating and cooling rates scale with the density and the density squared, respectively. In addition, for the same physical extent of the envelope the total extinction scales with the density. For $n_0 = 3.5 \times 10^5$ cm^{-3}, the 100 K region is confined to the inner 150 AU with approximately the same peak temperature as for the generic model, while for $n_0 = 3.5 \times 10^3$ cm^{-3} the peak temperature reaches 250 K and temperatures larger than 75 K are found throughout the envelope up to 3000 AU. Variations in the density power-law index between -0.5 and -2.0, corresponding to that of a singular isothermal sphere, yield similar variations for the extent of the warm region as found for the changes in n_0. Although the maximum kinetic temperature and the distribution of warm gas changes with density n_0 and density power-law index, the total amount of warm gas remains roughly constant. Therefore, the intensity of the optically thin ^{13}CO lines is insensitive to variations in these parameters. The strength of the optically thick ^{12}CO lines decreases with increasing n_0 or steeper density power-law, as the beam filling factor of the warm gas decreases.

Because the emergent intensities are not a strong function of the assumed parameter values for quite a large region of parameter space, it is not surprising that comparable mid-J CO line intensities are found toward a large number of different sources. In addition, the presence of strong self-absorption in most CO 4–3 spectra (Fig. 4.3), and its absence in most CO 6–5 spectra is very well reproduced within the examined parameter range. By changing the source orientation from edge-on to pole-on, the CO line intensities increase by a factor ~ 2, while the depth of the self-absorption feature in the CO 4–3 spectra decreases, and disappears close to pole-on.

4.4 TMR 1 as an example

^{12}CO and ^{13}CO 6–5 spectra toward TMR 1 were obtained in a 11$''$ (1500 AU) beam with the Caltech Submillimeter Observatory (CSO)[1] in December 1994 using the SIS receiver of Kooi et al. (1994). ^{12}CO 4–3 spectra were obtained in a similar beam in the same period using the James Clerk Maxwell Telescope (JCMT)[2] with the facility receiver C2. Limited maps were obtained in all lines. The spectra are presented in Fig. 4.3 and have been corrected for main beam efficiency, with $\eta_{\rm mb}$ obtained from measurements of planets, at $\eta_{\rm mb} = 0.4$ (CSO) and $\eta_{\rm mb} = 0.55$ (JCMT). Further details are given in Chapter 3 (Hogerheijde et al. 1998a).

The data are compared with a model with $L_{\rm bl} = 1\ L_\odot$, $n_{\rm H_2} = 1.0 \times 10^5$ cm^{-3} at 1000 AU, inclination angle 45°, $V_0 = 1$ km s^{-1} and $b = 1$ km s^{-1}. As can be seen from these spectra the proposed heating mechanism successfully accounts for much of the observed, narrow, ^{12}CO and ^{13}CO 6–5 emission over 10$''$–20$''$ (1400–3000 AU) scales. Our model overestimates the ^{12}CO 4–3 emission since absorption by the colder, less dense foreground material in the surrounding quiescent cloud is neglected. Additional

[1] The Caltech Submillimeter Observatory is operated by the California Institute of Technology under funding from the U.S. National Science Foundation (#AST96–15025).

[2] The James Clerk Maxwell Telescope is operated by the Joint Astronomy Centre on behalf of the Particle Physics and Astronomy Research Council of the United Kingdom, the Netherlands Organization for Scientific Research and the National Research Council of Canada.

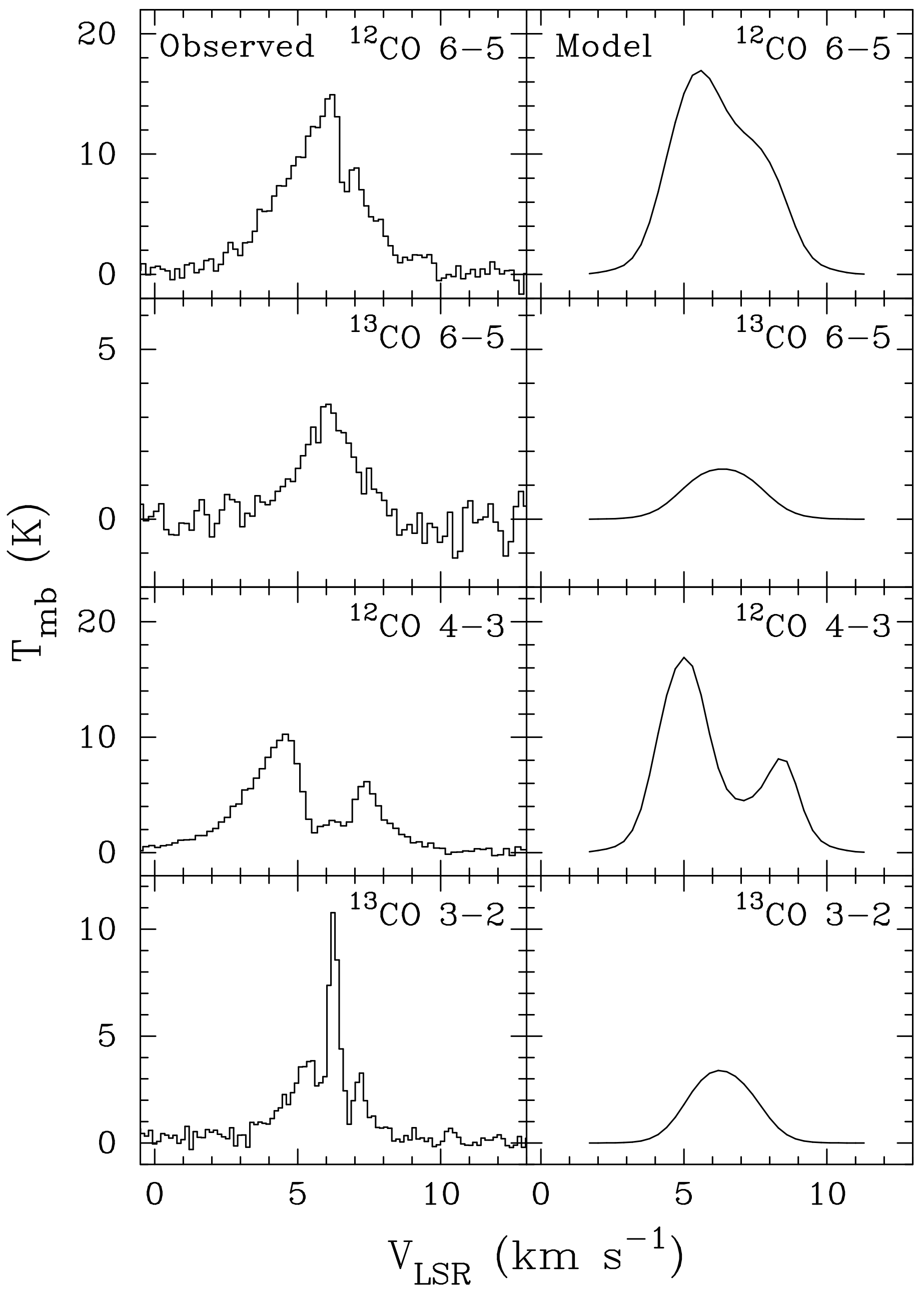

Fig. 4.3. *Observed (left) and modeled (right) spectra of TMR 1. From top to bottom: ^{12}CO 6–5, ^{13}CO 6–5, ^{12}CO 4–3 and ^{13}CO 3–2 spectra, convolved with respective beams of 11″, 11″, 11″ and 13″ FWHM, corresponding to 1500 AU at the distance of Taurus. An inclination angle of 45° is assumed for the source.*

emission due to molecular material entrained in the outflow is present in the ^{12}CO line wings, especially on the blueshifted side. No attempt has been made to reproduce the line profiles in great detail by fine-tuning the parameters V_0 or inclination.

This work demonstrates that mid–J CO line emission can be generated by cool PDRs around low-mass YSOs. A 10,000 K boundary layer and a small amount of dust in the outflow cavity will lead to ^{12}CO and ^{13}CO 6–5 emission with narrow line width and brightness temperatures of 10–20 K and 0.5–5 K respectively over 1400–3000 AU regions. These results are comparable in strength and extent to observed CO 6–5 emission toward a number of embedded sources in Taurus, though some contribution from the outflows is evident in the ^{12}CO line wings. The proposed mechanism operates irrespective of the presence of slow, $V_s = 5 - 10$ km s^{-1}, or oblique, C-type shocks along the outflow cavity walls, which could generate comparable amounts of emission (Draine & Roberge 1984). Only careful modeling of the line excitation and profile shapes can distinguish both contributions, requiring detailed knowledge of the gas density distribution and kinematics.

Acknowledgments The authors thank the referee for suggesting many improvements in the presentation of the paper. They are indebted to Geoff Blake for the CSO observations and to the JCMT staff for their support during several observation runs. Lee Mundy acknowledges the hospitality of the Sterrewacht Leiden and a *bezoekersbeurs* from the Netherlands Organization for Scientific Research (NWO). Research in astrochemistry in Leiden is supported through a PIONIER grant from NWO.

Note: The work presented in this chapter preceded much of the analysis of Chapter 2, and the details of the model for TMR 1 adopted here differ somewhat from the ones inferred in that chapter. This does not affect any of our conclusions.